Harsh Environment Sensor Array-Enabled Hot Spring Mapping

Jonathon Oiler, *Member, IEEE*, Everett Shock, Hilairy Hartnett, Andrew J. Dombard, and Hongyu Yu, *Member, IEEE*

***Abstract*— We report the design, fabrication, and application of temperature and electrical conductivity sensor arrays for studying the harsh environments of hot springs at Yellowstone National Park. Centimeter-scale measurements are necessary to measure sharp gradients in geochemical parameters across the photosynthetic/nonphotosynthetic transition zone known as the photosynthetic fringe. Platinum, parylene-C, and fused quartz were the critical materials used in fabrication of both sensor arrays. More than 700 temperature and 90 conductivity measurements were taken in the mixing zone, where two geochemically distinct hot spring channels converged. We present a new technique, whereby microscale temperature measurements can be used to predict ion concentrations that represent the bulk ion chemistry via electrical conductivity (or other conservative chemicals) in this mixing zone. High-spatial-resolution data confirm that the strong temperature gradients across these regions largely determine where photosynthetic organisms appear.**

***Index Terms*— MEMS, sensors, harsh environment, arrays, temperature, electrical conductivity.**

Fig. 1. Water from a hot spring source pool (upper right, dark blue) spills over and flows down the outflow channel toward the viewer. Total width of outflow channel is ∼1.5m. Note the sharp transition in the appearance of photosynthesis where the color changes from off-white to bright green.

I. Introduction

HOT spring ecosystems are some of the harshest inhabited environments on Earth. Hot springs occur when meteoric water is circulated through high-temperature rock; typically, hot rock surrounds magma chambers associated with volcanic activity or occurs in tectonically active regions. The water is delivered back to the surface at very high temperatures (∼100 °C). Large amounts of emerging water can form source pools. Water that rises above the rim of the source pool can spill out and form an outflow channel that carries water away from the source. These outflow channels host a diverse array of micro-organisms, from chemosynthetic microbes in the hottest zones nearest the source to photosynthetic bacteria and eukarya in lower temperature regions farther away from the source [1]. The appearance of photosynthesis in the hot springs can be sudden and dramatic (Fig. 1).

In-situ measurement of temperature across the transition zones between chemosynthetic and photosynthetic microbial communities, or between different photosynthetic microbial communities in hot springs, can be ambiguous using current robust bulk measurement techniques due to the small spatial scale of the transitions. Outflow channels are often narrow and shallow as they transport water away from the source pool, creating additional constraints on the size of the instrument and measurement technique used [2]. The transition zones where photosynthetic bacteria appear can occur in less than a few centimeters [3]. Therefore, high spatial resolution measurements are necessary to understand the parameters driving this transition.

Micro-Electro-Mechanical Systems (MEMS) technology is well-suited for making field-based temperature and conductivity measurements such as in the ocean [4], however, they have not previously been designed for use in hot springs. Advances in materials and fabrication techniques have enabled the development of chemically and thermally tolerant sensors suitable for more harsh environments [5]. The small size of the sensing elements provides the high spatial resolution

Manuscript received March 30, 2014; revised May 28, 2014; accepted June 17, 2014. Date of publication August 1, 2014; date of current version August 18, 2014. This is an expanded paper from the IEEE SENSORS 2013 Conference. The associate editor coordinating the review of this paper and approving it for publication was Prof. David A. Horsley.

J. Oiler was with the School of Earth and Space Exploration, Arizona State University, Tempe, AZ 85287 USA. He is now with the Space and Naval Warfare Systems Center-Pacific, San Diego, CA 92152 USA (e-mail: jonathon.oiler@navy.mil).

E. Shock is with the Department of Chemistry and Biochemistry, School of Earth and Space Exploration, Arizona State University, Tempe, AZ 85287 USA (e-mail: eshock@asu.edu).

H. Hartnett is with the Department of Chemistry and Biochemistry, School of Earth and Space Exploration, Arizona State University, Tempe, AZ 85287 USA (e-mail: h.hartnett@asu.edu).

A. J. Dombard is with the Department of Earth and Environmental Sciences, University of Illinois at Chicago, Chicago, IL 60607 USA (e-mail: adombard@uic.edu).

H. Yu is with the School of Earth and Space Exploration, School of Electrical, Computer, and Energy Engineering, Arizona State University, Tempe, AZ 85287 USA (e-mail: hongyuyu@asu.edu).

Color versions of one or more of the figures in this paper are available online at http://ieeexplore.ieee.org.

Digital Object Identifier 10.1109/JSEN.2014.2334674

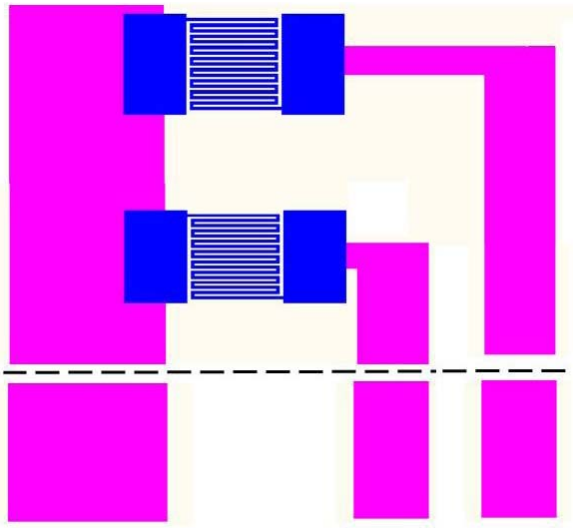

Fig. 2. Layout showing two Ni RTDs (blue) in an array (not to scale). The RTDs share a common 300 nm thick Cu ground lead (left pink lead). The dashed line represents a break in the design to show the bond pad alignment at the bottom of the array.

necessary to interrogate the sharp transition zones between chemosynthetic and photosynthetic organisms. Owing to the small size of each sensor and the ability to batch-fabricate many sensors at once, arrays of temperature and electrical conductivity sensors were fabricated. Electrical conductivity provides a method for characterizing the bulk ion chemical content within the hot spring fluids. The linear temperature array consisted of 15 temperature sensors with separations of 1 cm. The linear conductivity array consisted of 5 conductivity sensors with separations of 1 cm. Micro-temperature and conductivity sensors have been developed previously for ocean environments

II. Sensor and Circuit Design

A. Sensor Design

The resistance temperature detector (RTD) [6] array was designed as a linearly arranged set of meandering resistors of length 350 μm and width of 10 μm (Fig. 2). The array was fabricated on a fused quartz substrate and the fabrication flow process is shown in Figure 3. Linearly arranged RTDs were patterned in photoresist, followed by electron-beam (e-beam) deposition and lift-off of 10 nm titanium (Ti) and 110 nm nickel (Ni). Nickel was chosen for its high temperature coefficient of resistance (TCR) (~6400 ppm/°C). The resistances of the Ni RTDs were 1100–1500 Ω. Next, leads connecting the resistors to the bond pads were patterned in photoresist, followed by e-beam deposition and lift-off of 20 nm chromium (Cr) and 300 nm copper (Cu). The Cu thickness was determined so that the leads contributed to <1% of the total resistance of the Ti/Ni RTDs. A 20 μm layer of Parylene-C was conformally deposited over top the entire structure. The last fabrication step (not shown in Fig. 3) involved patterning and removing the Parylene-C over the Cr/Cu bond pads using an O_2 plasma etch.

Electrical connections were made to the bond pads via soldering 30 AWG wires. These wires were insulated with

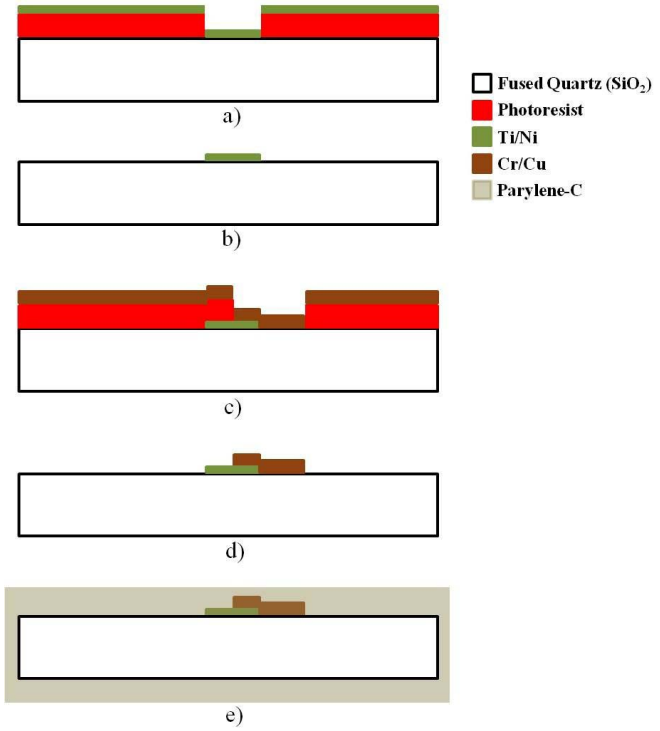

Fig. 3. A schematic of the fabrication of the fused quartz substrate temperature array in cross-section. A layer of Ti/Ni is deposited and patterned on the Si wafer to create the resistor in (a) and (b). Next a layer of Cr/Cu is deposited and patterned to create the bond pads and leads connecting pads to the resistors in (c) and (d). Finally, Parylene-C is deposited over the entire wafer in (e).

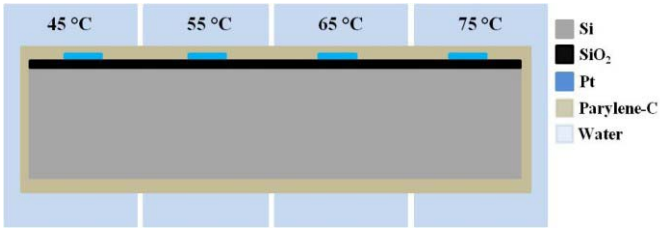

Fig. 4. Schematic of silicon substrate RTD array simulated with Comsol Multiphysics® heat transfer package (not to scale).

PTFE for protection from the corrosive hot spring fluids. An electrically insulating epoxy (H77, Epoxy Technologies) was placed over the solder connections to increase strength. The entire array was coated with a second layer of 20 μm Parylene-C to provide additional protection.

Parylene-C was ideally suited for these applications due to its inertness to a wide range of pH conditions, low water leakage rate, and biocompatibility [7]. Initially, the RTD array was fabricated on a silicon substrate with a thin film of silicon dioxide (SiO_2) for electrical insulation. However, data collected from the field showed smaller measured temperature gradients than were expected. Therefore, the RTD array was modeled using Comsol Multiphysics (Fig. 4) where the thicknesses were: Si – 500 μm, SiO_2 – 500 nm, Platinum (Pt) –100 nm, Parylene-C – 20 μm. Platinum (instead of nickel) was modeled as the RTD metal based on a previous design and does not change the result. Four water reservoirs of different temperatures were placed over four linearly arranged RTDs.

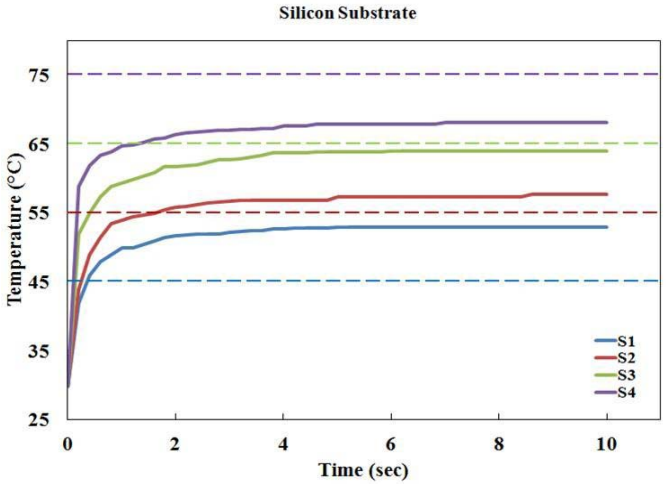

Fig. 5. Comsol model results for the silicon substrate RTD array. Solid lines show the temperature at the center of the metal resistors under heating from reservoirs of water at 45 °C, 55 °C, 65 °C, and 75 °C, which are represented by the dashed lines. The unit of time on the x-axis is seconds. The dashed lines of the same color with the solid lines show which water reservoir temperature is associated with each resistor.

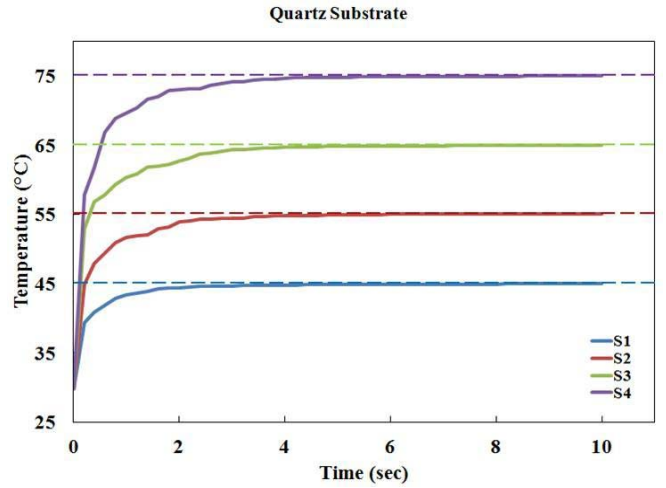

Fig. 6. Comsol model results for the fused quartz substrate RTD array. Solid lines show the temperature at the center of the metal resistors under heating from reservoirs of water at 45 °C, 55 °C, 65 °C, and 75 °C, which are represented by the dashed lines. The unit of time on the x-axis is seconds. The dashed lines of the same color with the solid lines show which water reservoir temperature is associated with each resistor.

The temperature of the RTD was simulated to steady-state. The separation between adjacent RTDs was 5 mm.

Results from the model showed that the RTDs' temperatures were different from the water reservoirs they sat in. The RTDs at the cold end were warmer than their respective reservoirs, and the RTDs at the hot end were cooler than their respective reservoirs, resulting in a smaller overall measured temperature gradient (Fig. 5). To solve this problem, the model was changed by replacing the Si substrate with fused quartz to take advantage of its low thermal conductivity, which is two orders of magnitude less than that of Si. Additionally, the 500 nm layer of SiO_2 was removed as it was no longer necessary. Results showed that the modified RTD temperatures matched the temperatures of the water reservoirs they sat in (Fig. 6). Based on these results, the original design was changed to reflect the design shown in Fig. 3.

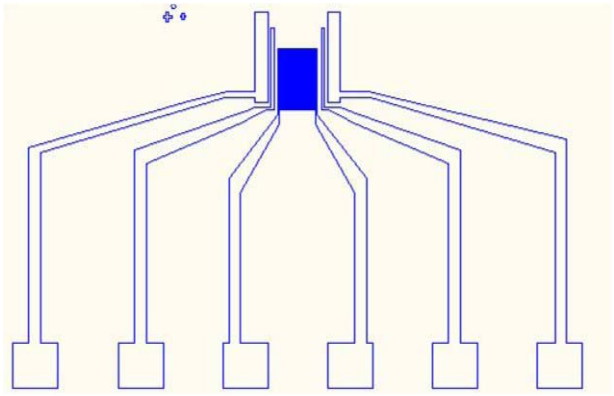

Fig. 7. Layout of a single four-point-probe conductivity sensor. The outer electrodes have a length of ∼1500 μm and width of ∼200 μm. The inner electrodes have a length of ∼1000 μm and a width of ∼50 μm. Spacing between the outer electrodes is ∼1000 μm and between the outer and inner electrode is ∼50 μm. The blue square in the center is an unresolved meandering RTD of ∼1000 Ω.

The conductivity sensors were designed as four-point-probes with electrode spacing optimized for the range of conductivities expected to be encountered in the field. The four-point-probe configuration utilized two outer electrodes to pass a current and two inner electrodes to measure the voltage drop across the solution (Fig. 7). By knowing the current passed through the solution and the voltage drop across it, the resistance of the solution can be determined via Ohm's Law. The conductance is the inverse of the resistance and the conductivity can be determined from conductance through knowing the cell constant of the four-point-probe or conversely, by calibrating with standard conductivity solutions. The cell constant was designed to be ∼5 cm^{-1} following methods in [8]. The four-point-probe configuration was ideal for minimizing measurement error resulting from resistance contributions from the leads. Platinum was required to minimize corrosion as the electrodes were directly exposed to the hot spring fluid. In addition, the platinum served to decrease the measurement error associated with polarization impedance [9].

The fabrication flow process for the conductivity sensor is shown in Figure 8. Photoresist was deposited and patterned to form the electrode, lead, and bond pad geometry and was followed by e-beam deposition of 10 nm Ti and 110 nm Pt and subsequent lift-off. The innermost (middle) platinum structure shown in the figure is a meandering RTD used for measuring temperature at the location of the conductivity measurement. Next, a 10 μm layer of Parylene-C was conformally deposited over top the entire structure. Photoresist is deposited and patterned over the four electrodes and all of the bond pads. The Parylene-C is then selectively etched with O_2 plasma. The central RTD is left covered by the Parylene-C and thus is not exposed to the fluid. Electrical connection was made to the bond pads via soldering 30 AWG PTFE insulated wires. The same electrically insulating epoxy was placed over the solder connections to increase strength. The entire system was coated with a second layer of 20 μm Parylene-C to provide additional

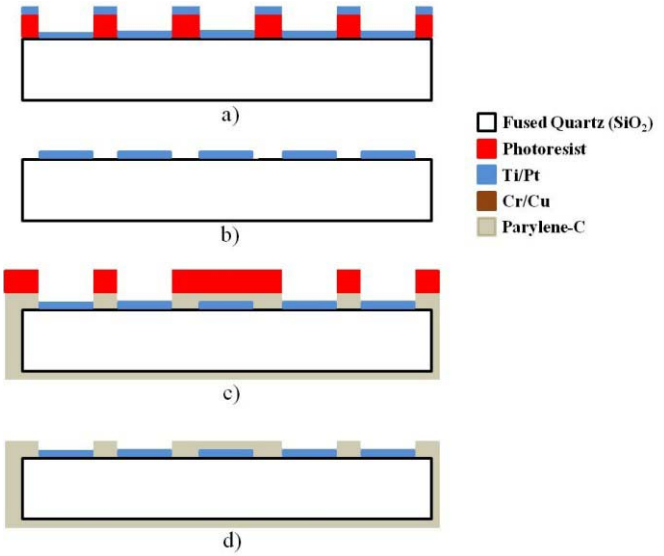

Fig. 8. Schematic of the fabrication process flow for the conductivity array in cross-section. Ti/Pt is deposited and patterned in (a) and (b). A layer of Parylene-C is deposited and selectively etched over the electrodes and bond pads in (c) and (d).

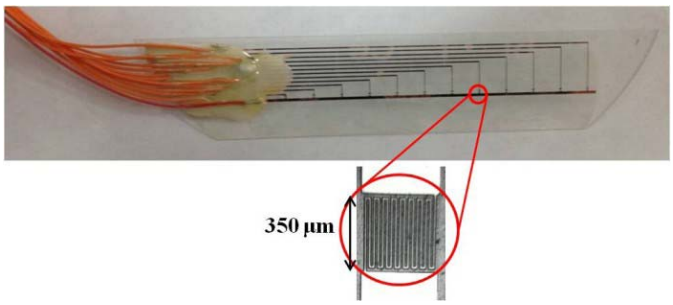

Fig. 9. Nickel-resistor temperature sensor array with 12 sensors fabricated on a fused quartz substrate and covered by Parylene-C. A magnified image of one of the RTD resistors with a meandering geometry is also provided.

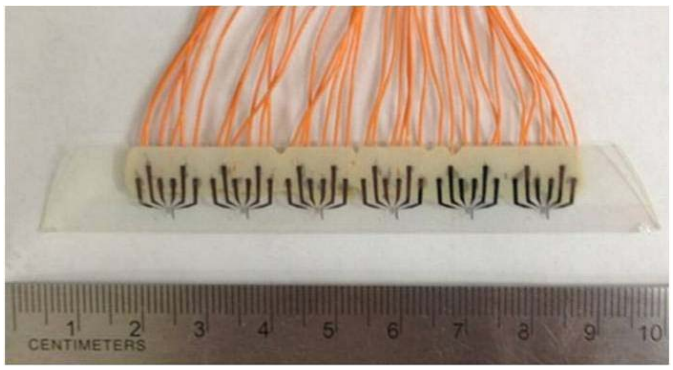

Fig. 10. Platinum electrode four-point probe electrical conductivity array consisting of six sensors.

protection. Kapton® tape was used to prevent Parylene-C deposition on the electrodes.

The electrodes were cleaned in an isopropyl alcohol solution after the tape was removed. Figure 9 shows a picture of a 12-RTD array along with magnified image of one of the meandering resistor RTDs. Figure 10 shows a 6-electrical conductivity sensor array. The RTD array was calibrated using a temperature controlled bath with ±0.2 °C error.

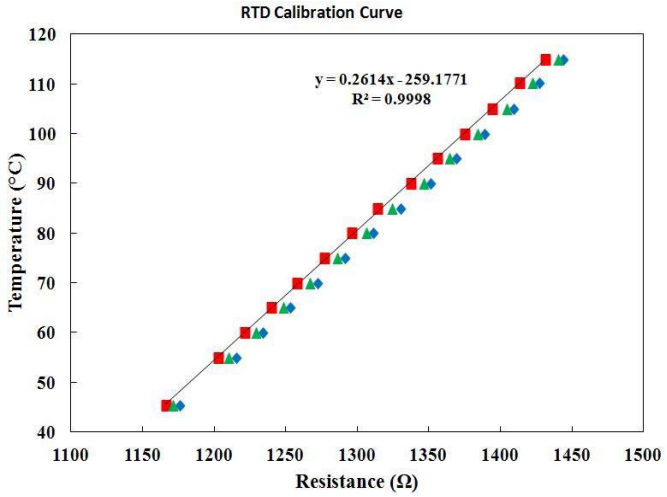

Fig. 11. Calibration curves of three RTDs on the same array. The TCR of the Ni RTDs was calculated to be ∼3260 ppm/°C.

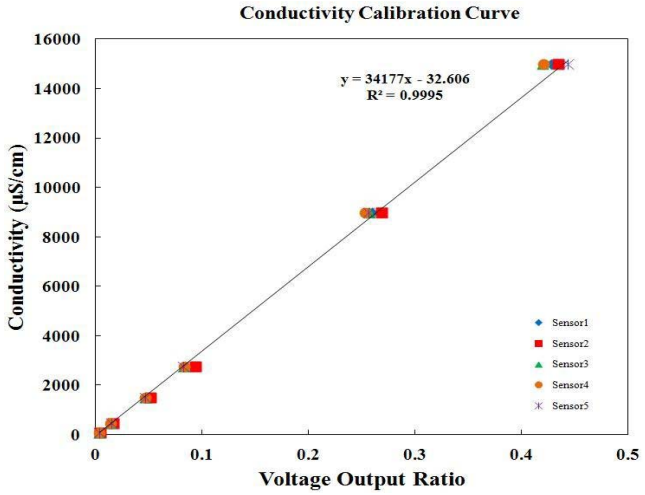

Fig. 12. Calibration curves for five conductivity sensors on the same array.

An example calibration curve of three adjacent RTDs on an array is provided in Figure 11. The TCR of these RTD (∼3260 ppm/°C) is lower than the theoretical Ni TCR due to the low Ni film thickness and deposition process conditions [10]. With additional noise and environmental constraints, the total measurement error was conservatively set to ±1 °C. The electrical conductivity array was calibrated using standard conductivity solutions between 84 μS/cm and 15000 μS/cm (standard solutions, Cole-Parmer) at room temperature and the measured error was conservatively set to ±10%. An example calibration curve is provided in Figure 12. The cell constant was measured to be ∼3.5 cm^{-1}. This value is different from the expected value (∼5 cm^{-1}) and is most likely due to small variations in the design geometry and electronic component values.

B. Circuit Design

For the temperature array, a circuit was designed and constructed to monitor the variable resistance values of the RTDs. Using Ohm's law, the current through the RTD and voltage drop across it must be known in order to determine

its resistance. Measuring the voltage drop across the RTD was carried out with a data acquisition device (USB-6289, National Instruments). The current flow through the RTD was measured indirectly, using another resistor in series with the RTD.

In this circuit, the source voltage (V_{source}) of 2 V was generated by the data acquisition device. The voltage magnitude was set so that the current through the RTD was high enough to be easily measured above the noise floor, but low enough so that it did not cause Joule heating. The relevant equations for solving for the RTD resistance are determined via Ohm's Law:

$$\frac{V_1}{V_{Source}} = \frac{\mathrm{R_{const}}}{\mathrm{R_{RTD}} + \mathrm{R_{const}}} \quad (1)$$

$$\frac{V_2}{V_{Source}} = \frac{\mathrm{R_{RTD}}}{\mathrm{R_{RTD}} + \mathrm{R_{const}}} \quad (2)$$

and finally $\mathrm{R_{RTD}}$ can be determined by dividing equation (2) by equation (1) and solving:

$$R_{RTD} = \frac{\mathrm{V_2}}{\mathrm{V_1}}\mathrm{R_{const}}. \quad (3)$$

The assumption that the constant resistance holds is critical to the accuracy of the RTD resistance measurement. Store-bought carbon-film resistors of a certain value typically have a tolerance of 5% and can have TCRs of 150-500 ppm/°C. Therefore a 10 000 Ω carbon film resistor may actually be anywhere from 9500-10 500 Ω and may change 5 Ω/°C. Because these resistors are directly in contact with the air around the hot spring and indirectly in contact with the ground near the hot spring, they can easily be warmed 10–15 °C above the temperature in the laboratory where they were calibrated. A 10 °C increase in the constant resistor temperature would result in a 50 Ω resistance increase that could cause the RTD hot spring temperature measurement to be undervalued by >1 °C (assuming a RTD value ~1200 Ω). This environmentally-induced error is far too high considering the additional error sources and the design requirement to have a measurement accurate to ±1 °C. Therefore, high precision/low TCR (10,000 Ω) resistors with a tolerance of 0.01% (±1 Ω) and TCR of ±10 ppm/°C (which is a resistance change of 1 Ω with a 10 °C increase in temperature) were used (Vishay Intertechnology, Inc., MR10210K000TAE66). With these resistors, a 10 °C increase in the environmental temperature would result in the hot spring temperature measurement undervalued by only 0.1 °C. This circuit is for one RTD and must be repeated for the number of RTDs in the array, although a common source voltage can be shared.

For the electrical conductivity array, the sensor configuration was designed to measure the resistance of the fluid. As mentioned previously, the four electrode design minimizes the resistance contributions from the leads and the choice of platinum for the electrode material minimizes the error associated with polarization impedance. Again, using Ohm's Law, the resistance was determined by knowing both the current through the solution and the voltage drop across the solution. The four-point-probe incorporates two outer 'force' electrodes for passing the current through the solution and two inner 'sense' electrodes for directly measuring the voltage drop across the solution.

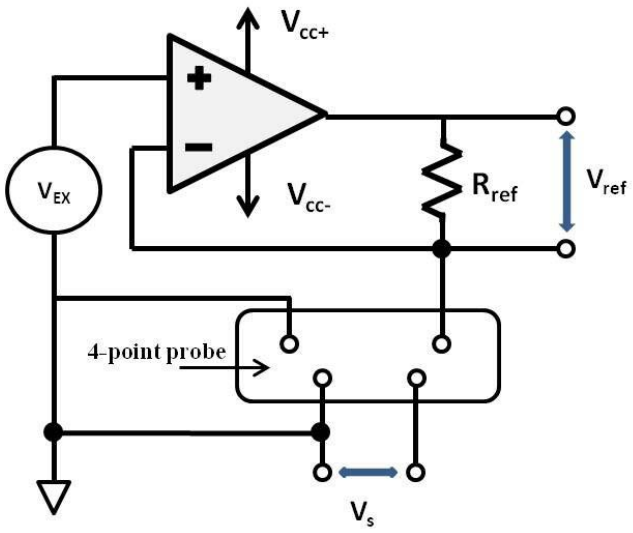

Fig. 13. Circuit schematic to measure the electrical conductivity of the solution in which the four-point-probe is immersed.

A circuit was designed (Fig. 13) following the methods presented in [11]. An alternating current is required for the input excitation signal in order to prevent electrolysis. Additionally, operating at higher frequencies can further reduce the impact of the polarization impedance. The excitation voltage (V_{EX}) was a 2 V peak-to-peak amplitude sinusoidal signal with a frequency of 1000 Hz and was generated by the data acquisition device.

The operational amplifier (ON Semiconductor, MC33079PG) was set up in a non-inverting configuration. In this configuration, the negative terminal of the operational amplifier has extremely high input impedance so the current flowing through the known resistor (R_{ref}) is the same current being passed through the hot spring fluid via the outer force electrodes. The value of the current was determined by measuring the voltage drop (V_{ref}) across R_{ref}. The voltage drop (V_S) across the solution of unknown resistance is measured by the inner sense electrodes. Once the resistance of the solution is determined, the conductance is determined by taking the inverse. In order to translate from conductance to conductivity, the cell constant of the sensor is needed; however, this step was bypassed by calibrating the sensors with solutions of known conductivity.

III. Results

Both the temperature and electrical conductivity sensor arrays were deployed in hot springs at Yellowstone National Park, USA. At one site, two geochemically distinct hot spring outflow channels converged. One channel was acidic (pH ~3.3, temperature ~36 °C, conductivity ~900 μS/cm). The second channel was alkaline (pH ~7.8, temperature ~60 °C, conductivity ~4200 μS/cm). Within a 15 cm wide section of the mixing zone, four distinctly colored photosynthetic microbial communities appear as striped features in the sediments that do not appear anywhere else in either of the two streams (Fig. 14).

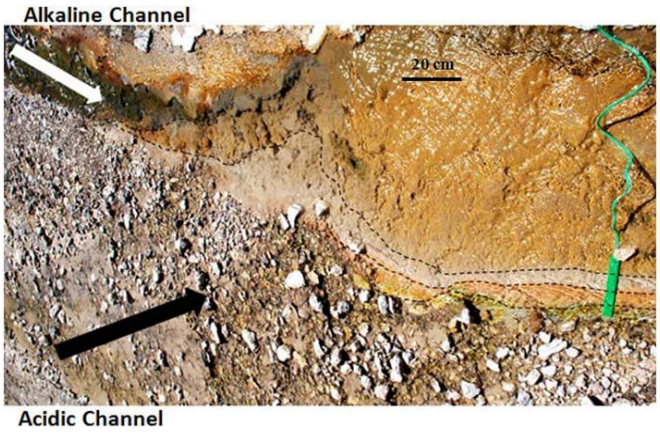

Fig. 14. Photograph showing the confluence of two hot spring outflow channels. Where the alkaline channel (top – white arrow) and the acidic channel (bottom – black arrow) mix, distinct bands of pigment are observed. The lines dividing the pigments are shown with dashed lines.

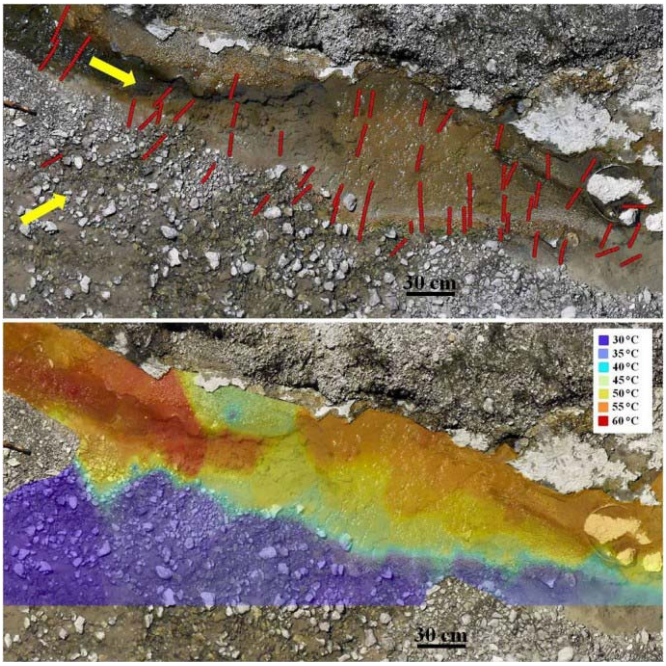

Fig. 15. (Top) Close-up image of the mixing zone where the two hot spring outflow channels merge. Red dots represent temperature measurements. The acidic stream is flowing in the direction of the bottom left yellow arrow and the alkaline stream is flowing in the direction of the top left yellow arrow. (bottom) Close-up of the temperature color map overlaid on the image.

More than 700 temperature and 90 conductivity measurements were taken within the mixing zone of the two geochemically distinct hot spring outflow channels using the sensor arrays in a single afternoon. The sensor arrays enabled the large number of temperature and conductivity measurements that were not otherwise achievable using existing measurement techniques.

Results of centimeter-scale high resolution mapping of temperature and conductivity in the mixing zone produced data that were used to create temperature and conductivity color maps using the ArcMap software [12]. The temperature color map traces out distinct regions that match the shape and width of many of the pigmented bands (Fig. 15). Color data between measurements were interpolated using the inverse distance weighting method.

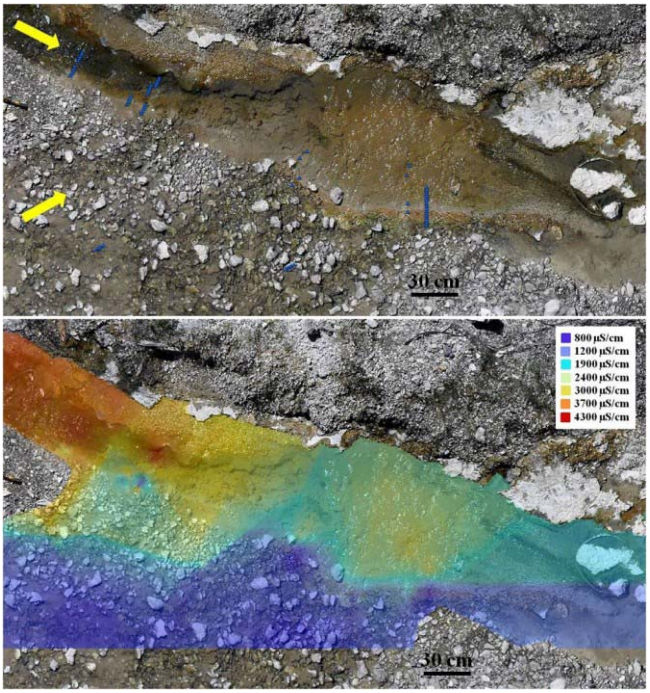

Fig. 16. (Top) Close-up image of the mixing zone where the two streams merge. Blue triangles represent conductivity measurements. The acidic stream is flowing in the direction of the bottom left yellow arrow and the alkaline stream is flowing in the direction of the top left yellow arrow. (bottom) Close-up of the conductivity color map overlaid on the image.

The electrical conductivity color map is shown in Figure 16. The conductivity data were too sparse to show any clear correlation with the colored photosynthetic regions. One obvious possibility is that conductivity has little effect on where the transition zones between photosynthetic communities occur in this system.

However, a qualitative comparison of the temperature and conductivity maps over areas where the conductivity and temperature sampling densities are both high shows that these areas correspond quite closely to the colored striping features of the microbial communities. Temperature and electrical conductivity data taken at the same location and measured across the photosynthetic stripes showed a similar structure (Fig. 17). Based on the structural similarity of the two plots, conductivity was modeled across the microbial striping zone using only temperature as a predictor.

In order to do this, the two streams were treated as end member reservoirs of a specific temperature and conductivity, and the mixing zone was treated as a linear combination of the end member reservoirs. The end member values for the temperature and conductivity of the acidic reservoir are $T_a = 36.7$ °C and $C_a = 890$ μS/cm, respectively. The end member values for the temperature and conductivity of the alkaline reservoir are $T_b = 59.9$ °C and $C_b = 4150$ μS/cm, respectively. The fractional contribution of water from each of the reservoirs can be determined at any location by knowing the temperature at that location (T_{mix}) via the following equations:

$$\mathrm{T_{mix}} = \mathrm{f_a T_a} + \mathrm{f_b T_b} \tag{4}$$

$$f_a + f_b = 1 \tag{5}$$

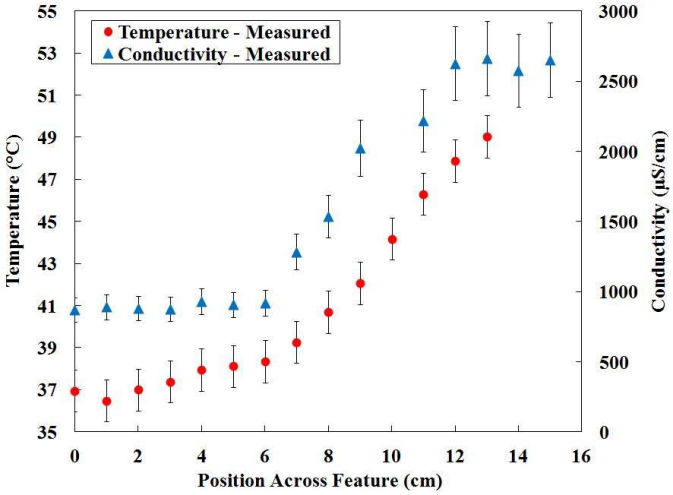

Fig. 17. Plot of the measured temperature and measured conductivity across the mixing zone at the same location.

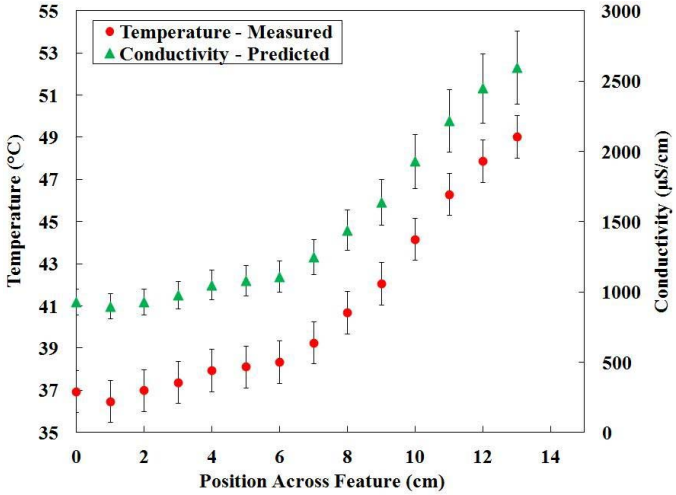

Fig. 18. Plot of the measured temperature and model-predicted conductivity across the mixing zone.

where f_a and f_b represent the fractional volumetric contribution of water from the acidic and alkaline reservoirs, respectively. Assuming there is no contribution other than that from the two reservoirs, the two fractions will add to unity. Using these fractions, the conductivity (C_{mix}) can be predicted at each location where the temperature was measured via

$$C_{mix} = f_a C_a + f_b C_b. \tag{6}$$

This method then acts to greatly increase the sampling density of the conductivity measurements. A plot showing the measured temperature and the model-predicted conductivity at the same location is provided in Figure 18. A plot of the measured conductivity and model-predicted conductivity is provided in Figure 19. The predicted and measured conductivity values match each other (within error), except for at one point.

Based on these results, it appears that a sampling density bias in the measured conductivity is the likely cause of the color discrepancies between the measured conductivity and temperature maps. Figure 20 shows the model-predicted conductivity color map, which has the same structure as the measured temperature map. Assuming the previous method holds true everywhere in the mixing zone, this conductivity color map provides a more representative view of the conductivity distribution across the mixing zone.

This also implies that conductivity (bulk ion chemistry) is a conservative constituent within this hot spring system. Conservative constituents are those elements or molecules whose concentration ratios relative to one another do not change and that are not noticeably affected by the presence of biological activity. This new technique may be extremely useful for predicting other conservative chemical parameters (those not influenced by biology or chemical reactions) such as elemental concentrations at high spatial scales impossible to measure at using existing water sampling techniques. The technique is limited to areas where there is mixing between two channels and where the temperature is governed by the mixing of the two fluids rather than another process such as evaporative cooling.

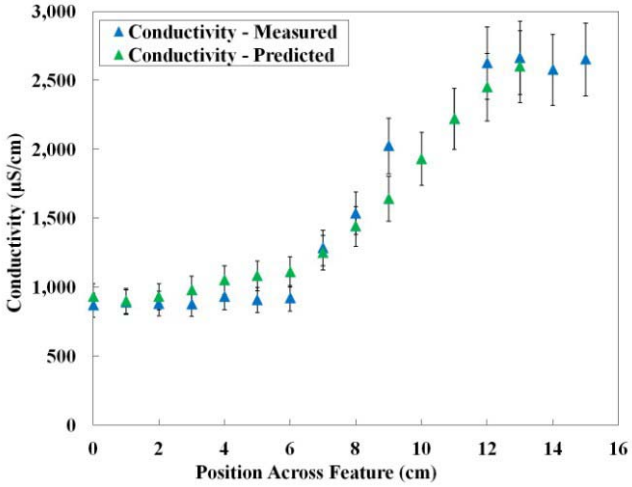

Fig. 19. Plot of the measured and model-predicted conductivity across the mixing zone.

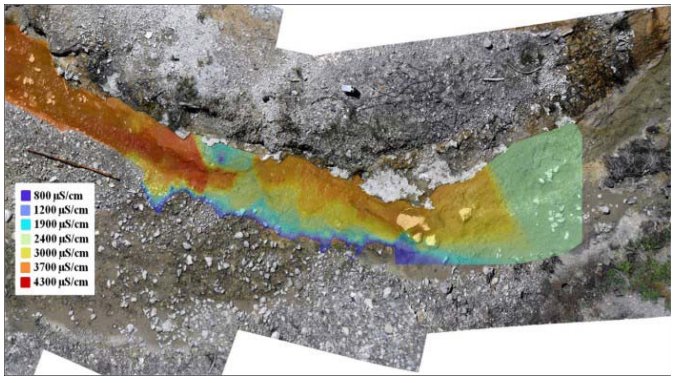

Fig. 20. Zoomed-out model-predicted conductivity color map of the acidic outflow mixing zone and alkaline channel (top of image). The stick above the scale bar is 1.2 m long for scale.

IV. Conclusion

The utility of MEMS sensor arrays to measure physical and chemical properties in a hot spring system has been shown. The large number of temperature and conductivity measurements taken would not have been possible using exist-

ing commercial technology. The system studied involved the mixing zone where two chemically distinct hot spring outflow channels merged. One channel was hot, alkaline, and had high conductivity, while the other was cool, acidic, and had lower conductivity. In the mixing zone where the two streams merged, a zone of several distinct photosynthetic microbial communities appears; these pigmented communities are not evident anywhere else in the two streams. A high resolution temperature color map was created using the high density temperature measurements collected with the sensor arrays. The spatial distribution of the various pigmented photosynthetic microbial communities could be traced based on the color (temperature zones) of the temperature map. In addition, a similar (albeit lower resolution) conductivity color map was created using the less dense conductivity array measurements.

Conductivity and temperature were compared across the mixing zone at approximately the same location and appeared to show the same trend. Therefore, the high-spatial-resolution temperature data were used to predict the conductivity based on a mixing model that assumed each stream was an end member reservoir of known conductivity and temperature. Model-predicted conductivity values matched the measured conductivity values fairly well at most locations. Therefore, the temperature data were used to create a high-resolution *model-predicted* conductivity color map. The ability to generate a high spatial resolution map of conductivity even though the measured data were sparse is a potentially powerful technique that could be utilized for other conservative constituents that are impossible to measure at those spatial scales.

ACKNOWLEDGMENT

The authors would like to thank Yellowstone National Park Service for permission to conduct research in the park.

REFERENCES

[1] S. M. Barns, R. E. Fundyga, M. W. Jeffries, and N. R. Pace, "Remarkable archaeal diversity detected in a Yellowstone National Park hot spring environment," *Proc. Nat. Acad. Sci. USA*, vol. 91, no. 5, pp. 1609–1613, Mar. 1994.

[2] J. P. Amend and E. L. Shock, "Energetics of overall metabolic reactions of thermophilic and hyperthermophilic Archaea and Bacteria," *FEMS Microbio. Rev.*, vol. 25, no. 2, pp. 175–243, Apr. 2001.

[3] A. Cox, E. L. Shock, and J. R. Havig, "The transition to microbial photosynthesis in hot spring ecosystems," *Chem. Geol.*, vol. 280, nos. 3–4, pp. 344–351, Jan. 2011.

[4] A. Hyldgard, D. Mortensen, K. Birkelund, O. Hansen, and E. V. Thomsen, "Autonomous multi-sensor micro-system for measurement of ocean water salinity," *Sens. Actuators A, Phys.*, vol. 147, no. 2, pp. 474–484, Jun. 2008.

[5] J.-M. Stauffer, B. Dutoit, and B. Arbab, "Standard MEMS sensor technologies for harsh environment," in *IET Seminar MEMS Sens. Actuators*, Apr. 2006, pp. 91–96.

[6] W. A. Clayton, "Thin-film platinum for appliance temperature control," *IEEE Trans. Ind. Appl.*, vol. 24, no. 2, pp. 332–336, Mar./Apr. 1988.

[7] J. Zhu *et al.*, "A novel technique to cover microfluidic systems with Parylene-C," in *Proc. 5th IEEE Int. Conf. NEMS*, Jan. 2010, pp. 840–843.

[8] D. He, "Theory, fabrication and characterization of micromachined electrolytic solution conductivity sensors," Ph.D. dissertation, Univ. Illinois Urbana-Champaign, Champaign, IL, USA, 2001.

[9] D. He, M. A. Shannon, and N. R. Miller, "Micromachined silicon electrolytic conductivity probes with integrated temperature sensor," *IEEE Sensors J.*, vol. 5, no. 6, pp. 1185–1196, Dec. 2005.

[10] A. Singh, "Film thickness and grain size diameter dependence on temperature coefficient of resistance of thin metal films," *J. Appl. Phys.*, vol. 45, no. 4, pp. 1908–1909, 2003.

[11] X. Li and G. C. M. Meijer, "A high-performance interface for grounded conductivity sensors," *Meas. Sci. Technol.*, vol. 19, no. 11, pp. 115202–115208, Sep. 2008.

[12] J. M. V. Hoef, K. Krivoruchko, and N. Lucas, *Using ArcGIS Geostatistical Analyst*, vol. 380. Redlands, CA, USA: ESRI, 2001, pp. 1–245.

Jonathon Oiler (M'07) received the B.S. degree in engineering mechanics (with an emphasis in astronautics), physics, and astrophysics from the University of Wisconsin-Madison, Madison, WI, USA, in 2007, and the Ph.D. degree in exploration systems design from Arizona State University, Tempe, AZ, USA, in 2013.

He was a Graduate Research Assistant in microelectromechanical systems (MEMS) with the Earth and Space Exploration Laboratory, Arizona State University, from 2007 to 2013. Since 2013, he has been a Civilian Research Scientist with the Department of Defense, Navy Government Laboratory, Space and Naval Warfare Systems Center-Pacific, San Diego, CA, USA. He has authored more than 10 articles, and more than 25 conference papers. His research interests include harsh environment sensors related to operating in hot and cold temperature environments, acidic and basic fluids, high salinity and high pressure environments, and MEMS devices utilizing resonators, chemical sensors, thermoelectrics, and flexible materials.

Everett Shock received the B.S. degree in earth sciences from the University of California at Santa Cruz, Santa Cruz, CA, USA, in 1978, and the Ph.D. degree in geology and geophysics from the University of California at Berkeley, Berkeley, CA, USA, in 1987. He was with Washington University in St. Louis, St. Louis, MO, USA, for 15 years, and presently holds a joint faculty appointment with the Department of Chemistry and Biochemistry and the School of Earth and Space Exploration, Arizona State University, Tempe, AZ, USA, where he serves as the Co-Director of the Transdiciplinary Environmental Life Sciences Graduate Program.

Hilairy Hartnett received the B.A. degree in chemistry from Vassar College, Poughkeepsie, NY, USA, in 1990, and the M.S. and Ph.D. degrees in oceanography from the University of Washington, Seattle, WA, USA, in 1995 and 1998, respectively. She is currently an Associate Professor with the School of Earth and Space Exploration, Department of Chemistry and Biochemistry, Arizona State University, Tempe, AZ, USA.

Andrew J. Dombard received the B.S. degree with a double major in physics and astronomy from Haverford College, Haverford, PA, USA, in 1994, and the Ph.D. degree in earth and planetary sciences from Washington University, St. Louis, MO, USA. He is currently an Associate Professor with the Department of Earth and Environmental Sciences, University of Illinois at Chicago, Chicago, IL, USA.

Hongyu Yu (M'08) received the B.S. and M.S. degrees in electronics engineering from Tsinghua University, Beijing, China, in 1997 and 2000, respectively, and the Ph.D. degree in electrical engineering from the University of Southern California, Los Angeles, CA, USA, in 2005. He joined the Arizona State University, Tempe, AZ, USA, in 2008, holding a joint position with the School of Earth and Space Exploration and the School of Electrical, Computer and Engineering. His research interests focused on microelectromechanical systems (MEMS) for earth and space exploration. His goal is to provide miniaturized portable platforms and instruments for scientists to explore variety of earth environments and space science, such as seismology, biogeochemistry, volcanology, and astrobiology. His current projects includes miniature seismometers for earth and moon exploration, flexible and stretchable shear stress sensor for river and hot spring monitoring, wireless radiation, UV and IR sensing, 3-D MEMS/NEMS manufacturing, origami electronics, and micro batteries.